Chemistry–A European Journal
Research Article
doi.org/10.1002/chem.202403245
Chemistry Europe
European Chemical Societies Publishing
www.chemeurj.org

Detection of Guanine Quadruplexes by Raman Optical Activity and Quantum-Chemical Interpretation of the Spectra

Mohammed Siddhique Para Kkadan,[a, b] Štěpán Jílek,[b] Václav Profant,[b] Josef Kapitán,[c] Jiří Kessler,[a] and Petr Bouř*[a]

Quadruplexes formed by guanine derivatives or guanine-rich nucleic acids are involved in metabolism and genetic storage of many living organisms, they are used in DNA nanotechnologies or as biosensors. Since many quadruplex geometries are possible the determination of their structures in aqueous solutions is difficult. Raman optical activity (ROA) can make it easier: For guanosine monophosphate (GMP), we observed a distinct change of the spectra upon its condensation and quadruplex formation. The vibrational bands become more numerous, stronger, and narrower. In particular, a huge ROA signal appears below 200 cm^{-1}. The aggregation can be induced by high concentration, low temperature, or by a metal ion. We focused on well-defined quadruplexes stabilized by potassium, where using molecular dynamics and density functional theory the spectra and particular features related to GMP geometric parameters could be understood. The simulations explain the main experimental trends and confirm that the ROA spectroscopy is sensitive to fine structural details, including guanine base twist in the quadruplex helix.

Introduction

Among building blocks of nucleic acids, guanine derivatives are exceptional in their ability to form self-assembled structures. The basic tetrameric – quadruplex - guanine arrangement in these aggregates was first described in 1962 for guanosine monophosphate (GMP),[1] and confirmed later for derived compounds.[2] GMP self-assemblies appeared as excellent models for the quadruplexes formed by guanine-rich nucleic acids in living cells.[3] These structures primarily attract attention in studies of metabolism and transfer of genetic information, although they can be found also in variable places of the living world. Interestingly, these often involve organs interacting with light, such as cuticles of spiders,[4] eyes of some deep-see fishes,[5] or chameleon skin.[6]

Apart from biology, the self-organization of noncovalent assemblies is of great interest in material science and nanoscience.[7] In spite of many previous efforts, however, the structure of GMP aggregates in solutions has not been unambiguously determined.[8] Therefore, its high Raman optical activity (ROA) observed for high-concentrated solutions of GMP potassium and sodium salts discussed in the present study appears as an extremely useful indicator of the quadruplex formation.

According to our knowledge, ROA has not been yet used to study guanine quadruplexes, although other low-resolution techniques are quite popular. For example, the self-association of purine nucleosides and guanosine salts was studied by nuclear magnetic resonance (NMR),[9] UV absorption and circular dichroism (CD) were used as well.[10] The quadruplex formation was also followed by vibrational circular dichroism (VCD) and unpolarized Raman spectroscopy.[11]

As shown below, ROA is not only sensitive to the formation of GMP aggregates, and also to their variants, such as sodium or potassium-stabilized structures. Specific changes are already observable in the parent Raman spectrum, but these are relatively minor. On the other hand, alterations of the ROA signal are more apparent: typically, the bands are narrower and gain in intensity. In particular, low-frequency ($<$ ~200 cm^{-1}) ROA signals become very strong. The strength itself in general broadens the application span of the spectroscopy, allowing measuring the spectra faster or in lower concentrations. Similar low-frequency signal was observed, for example, in polyalanine,[12] globular proteins,[13] or chiral liquids.[14] The GMP aggregation can be triggered by low temperatures, high concentrations, or presence of metal ions. Different aggregation conditions lead to different aggregates, and characterization of their variability goes far beyond the scope of the present work. Instead, we focus on the quadruplexes formed from potassium salts, which are presumably the most stable and cause distinct ROA changes.

[a] M. S. P. Kkadan, J. Kessler, P. Bouř
Institute of Organic Chemistry and Biochemistry, Academy of Sciences, Flemingovo náměstí 2, 16610 Prague, Czech Republic
E-mail: bour@uochb.cas.cz

[b] M. S. P. Kkadan, Š. Jílek, V. Profant
Institute of Physics, Faculty of Mathematics and Physics, Charles University, Ke Karlovu 5, 12116 Prague, Czech Republic

[c] J. Kapitán
Department of Optics, Faculty of Sciences, Palacký University Olomouc, 17. listopadu 12, 77146 Olomouc, Czech Republic

Supporting information for this article is available on the WWW under https://doi.org/10.1002/chem.202403245

We apply the most common scattered circular polarization (SCP) variant of ROA that monitors a small circularly polarized component in the scattered light.[15] In the past, ROA spectroscopy has been found particularly useful in studies of small chiral molecules,[16] peptides,[17] proteins,[18] and saccharides.[19] Many systems related to nucleic acids were investigated as well, including nucleosides, polynucleotides, and whole viruses.[20] Compared to the other form of vibrational optical activity, vibrational circular dichroism (VCD), ROA offers the possibility to easily work with water solution and capture a wider range of vibrational frequencies.

However, the interpretation of ROA spectra often relies on multi-scale molecular dynamics (MD) and density functional theory (DFT) simulations, which are particularly problematic for nucleosides, such as GMP. These molecules strongly interact with the aqueous environment, which necessitates a good modeling of the solvent.[21] Vibrational frequencies of various chemical entities – phosphate, aromatic, sugar – are calculated using DFT with different precision, which may distort the fine spectral pattern.[22] Finally, the steep dependence of the computational demands on molecular size prevents direct modeling of large aggregates, such as the quadruplexes.

To overcome these problems, we adopted various approaches. The dependence of the energy and spectra on the geometry was investigated on a simplified model lacking the sugar-phosphate part. Whole GMP quadruplex polymers where modeled using DFT, applied either on smaller regular fragments or ensemble of dimers obtained from MD. Vibrational parameters calculated for the smaller structures were transferred on bigger ones using the Cartesian coordinate-based tensor transfer.[23]

As shown below, such simulations provided useful information on system geometry and the origin of Raman and ROA spectral bands. Computed energies and spectral patterns reveal self-assembling principles of the guanine units and a favorable twist of G-quartets in the presence of potassium. Altogether, the results demonstrate the power of the combined computational and experimental spectroscopy to study the behavior of biomolecular systems.

Results and Discussion

Experimental Spectra

Figure 1a documents the changes under the 190 → 500 mM concentration variation of $GMPK_2$. Relatively small changes appear in Raman spectrum, such as new bands at 106 and 1724 cm^{-1}. The 106 cm^{-1} band seems to be composed of 96 and 112 cm^{-1} sub-bands. The 1724 cm^{-1} signal was assigned to formation of guanine-guanine hydrogen bonds.[24] A more detailed analysis also reveals new signals at 177 and 199 cm^{-1}, intensity drop at 1685 cm^{-1}, etc.

Unlike Raman, ROA bands become significantly more intense, numerous, and sharper. For example, the couplet (close positive and negative bands) at 1573/1586 cm^{-1} changes sign and increases intensity about five times, and a new one appears at 1457/1474 cm^{-1}. Most stunning is perhaps the region below 200 cm^{-1} where strong ROA bands (77, 97, 113, 134 cm^{-1}) grew up, from virtually zero GMP signal at the lower concentration. The Raman intensity here is also big, so the circular intensity difference (CID, ROA/Raman ratio) at this region is not extreme (~10^{-3}), but slightly above the average (~5×10^{-4}). As discussed before, the low-frequency ROA is usually associated with motion of whole molecules or molecular parts and significantly improves the detection limit and thus the application span of the ROA spectroscopy.[12,14]

Based on previous work we assign the spectral changes at higher concentration to a formation of quadruplex aggregates.[10] GMP salts of other metals (Na, Li, Rb, etc.) give ROA spectra similar in intensity but different in shape. As an example, low and high-frequency spectral parts of $GMPNa_2$ and $GMPK_2$ solutions are shown in Figures 1b,c for selected temperatures. For the aggregation of $GMPNa_2$ a higher concentration is needed (763 mM) and the aggregate is less stable at elevated

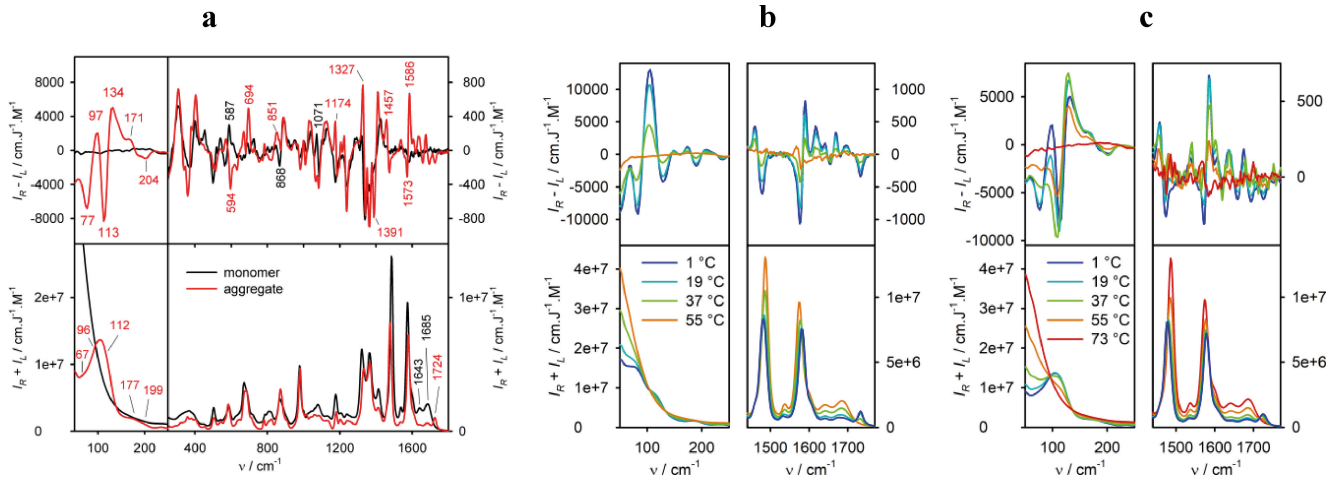

Figure 1. (a) Experimental ROA (I_R-I_L) and Raman (I_R+I_L) spectra of potassium salt of GMP at concentrations of 190 mM (monomer) and 500 mM (aggregate), 19 °C, (b) sodium 763 mM and (c) potassium 500 mM GMP salt solutions for several temperatures.

temperatures than for $GMPK_2$: while for sodium enhanced ROA disappears at 55 °C, for potassium typical monomer signal is not reached until around 70 °C.

Analyzing the fine metal effects goes beyond the scope of this work; nevertheless it is clear that this spectroscopy appears extremely useful for indication of the quadruplex formation. In this context, we view focusing on the most stable potassium structures as the first step in understanding the amazingly variable quadruplex aggregates.

Potential Energy Surfaces of the M Dimer Model

To understand the quadruplex aggregation, we found it useful to investigate behavior of symmetric dimers formed by a simplified quadruplex (M, Figure 2). In the figure, dependencies of the electronic energies on the distance and twist are plotted, for "regular" (C_4) and "flipped" (D_4) dimers.

The D_4 dimers were included for completeness, although they probably do not support longer regular polymers. From the energy maps we see that the presence of one (in the middle) or two (in the quadruplex plane) metal ions does not affect the basic behavior. Focusing on the regular (C_4) case we see that relatively well-defined minima exist for all cases, at d ~3.1–3.3 Å and τ~20/70°. Because of the symmetry, the M dimer cases of $\tau = 20°$ and $\tau = 70°$ represent right and left-handed enantiomers, respectively. For GMP, the symmetry can be obviously broken by the sugar-phosphate residue.

For the D_4 dimers, the stacking leads to less compact structures and the equilibrium distance is slightly bigger, d~3.20–3.40 Å. The addition of one metal ion to the dimers without ions leads to smaller stacking distances, thus stabilizing the dimer, while addition of two ions has more complex effects.

For further analysis, full optimization was performed for the potential energy minima at the B3LYP/6-311++G**/GD3BJ/CPCM(H_2O) level, resultant energies, and the geometrical

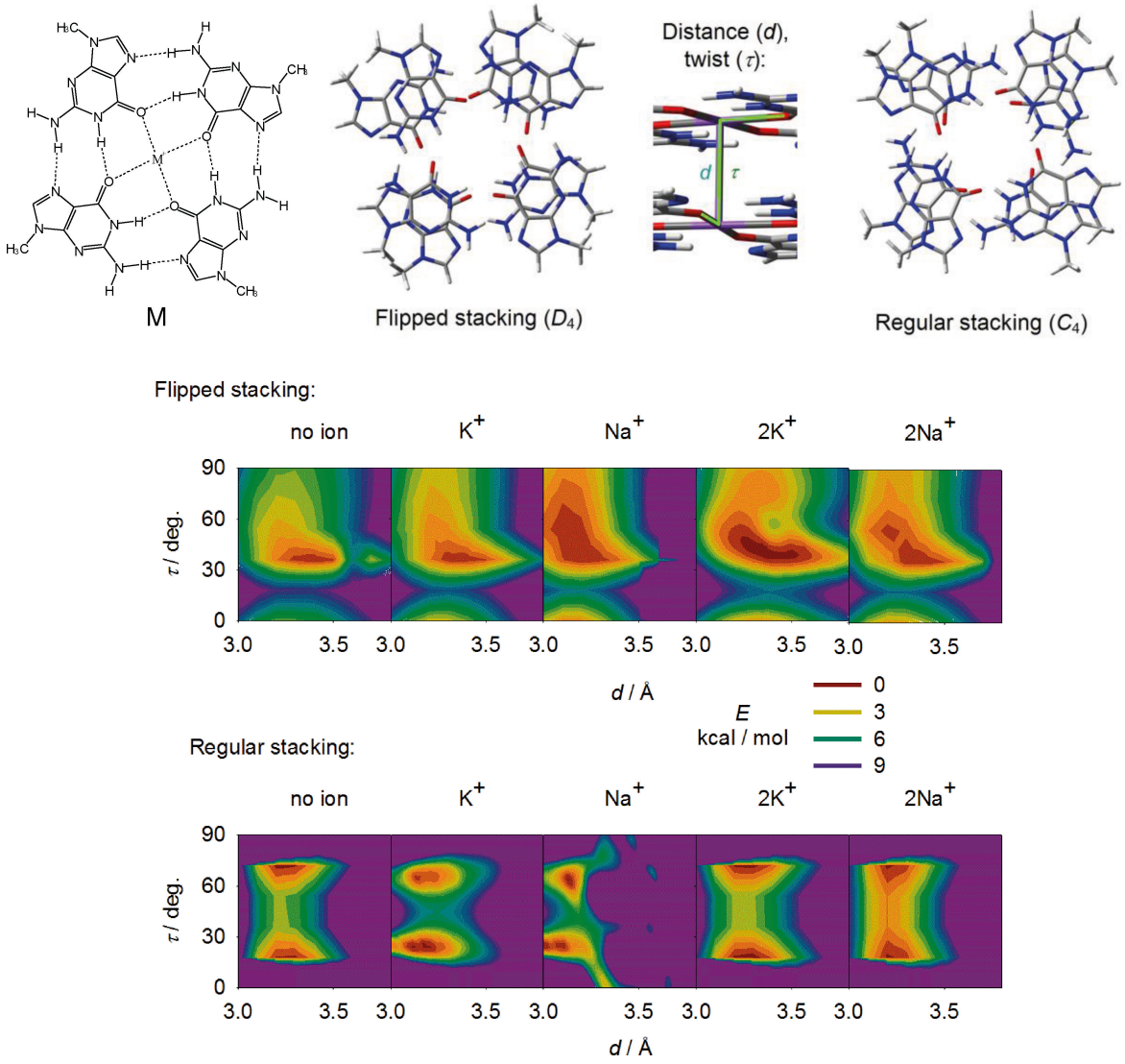

Figure 2. Model 9-methylguanine quadruplex ("M", with $M^+ = Na^+$ or K^+), flipped and regular stacking types in a dimer, characteristic distance and twist, and dependencies of relative electronic energy on the twist (τ) and distance (d), a B3LYP/6-31G**/GD3BJ/CPCM(H_2O) calculation.

parameters are listed in Table S1, the optimized geometries are plotted in Figure S1. The initial geometries favorable for a regular quadruplex polymer remain stable for bare dimers, and K^+ and Na^+ ions stay in the middle, except for the Na^+/C_4 case. Structures with two metal ions are stable, too, but cause significant deformations of the plane of the bases. Finally, the two metals behave differently. The larger potassium moves out farther from the G-quartet planes, but allows for C4 symmetry, while sodium stays closer to the plane approximately formed by the four purines. Sodium also makes the G-quartets to slightly glide off the symmetry arrangement, which could be related to the differences between the two metals observed in the experiment (Figure 1).

Contributions of Molecular Parts to the Spectra

The band assignment was aided by a computer experiment where some atomic polarizability derivatives were deleted and approximate contributions of individual molecular parts to Raman and ROA intensities estimated (Figure 3).

For monomeric GMP, consistently with a previous study,[22] the Raman signal above 1250 cm^{-1} is almost exquisitely formed by the guanine base, which significantly contributes to other parts of the spectrum as well. For ROA, the base contribution is rather minor, and the total signal is far from the sum of the three components. For the quadruplex (lower part of the figure), however, the ROA picture is entirely different. Above 1400 cm^{-1} and below 250 cm^{-1} the spectrum stems primarily from the guanine bases. The two quartets are virtually planar and do not produce inherent ROA. Therefore, we can ascribe the signal to the exciton coupling between them. This coupling of vibrations of similar frequencies often leads to very strong vibrational optical activity, typically conserved couplets, observed both in VCD[25] and ROA.[26] Above 1400 cm^{-1}, such vibrations include C=O stretching, N–H bending, and aromatic stretching, while below 250 cm^{-1} H-bonding and in- and out-of-plane deformation modes dominate (cf. Table S2 for detailed assignment).

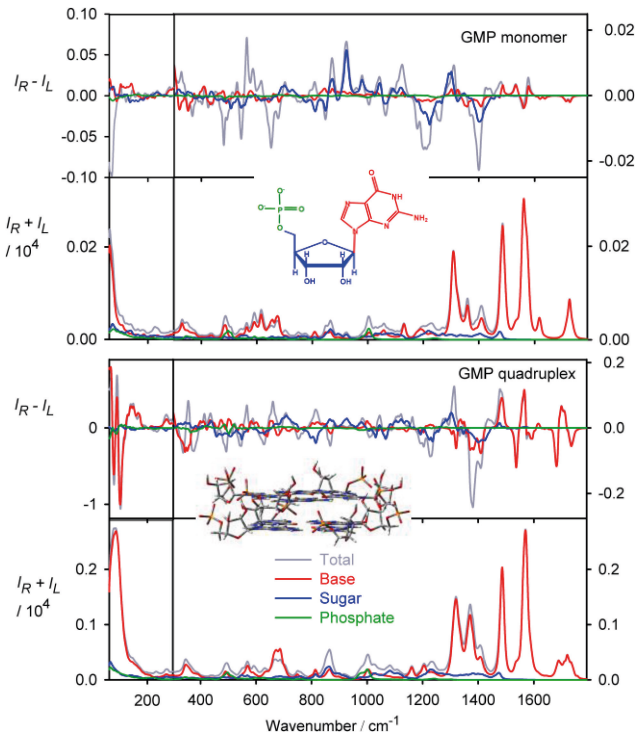

Figure 3. Contributions to Raman and ROA spectra calculated for individual GMP molecular parts, for (top) monomer and (bottom) octamer in a quadruplex dimer.

Spectra Signatures of the Bases

For frequency regions dominated by the guanine base, quadruplex spectral patterns could be conveniently investigated with the M model. Indeed, depending on the geometry, M dimers exhibit a huge ROA signal in the lowest wavenumber region, within ~50–200 cm^{-1}, corresponding to the observed spectra of concentrated solutions (Figure S2). For the D_4 structures, however, the calculated CID ratios are too high if compared with the experiment. As they also do not support regular quadruplex polymers, we suppose that they are rather rare in the measured samples.

The still strong, but not extreme low-frequency ROA calculated for the C_4 dimers is more realistic. In Figure 4 the low-frequency spectra simulated for the twist $\tau = 64°$ gives ROA pattern reasonably resembling the potassium experiment. Also above 1400 cm^{-1} this value provides a reasonable similarity to the experiment (Figure S3). In particular, the bands calculated at 72, 96, 117, and 131 cm^{-1} seem to correspond to the experimental ones respectively at 77, 97, 113, and 134 cm^{-1}, as their signs and relative intensities approximately agree. The assignment of the Raman experimental pattern is less obvious as it is rather less resolved, although also here the frequency of the most intense band at 106/108 cm^{-1} (exp./calc.) again seem to indicate that the modeling is realistic.

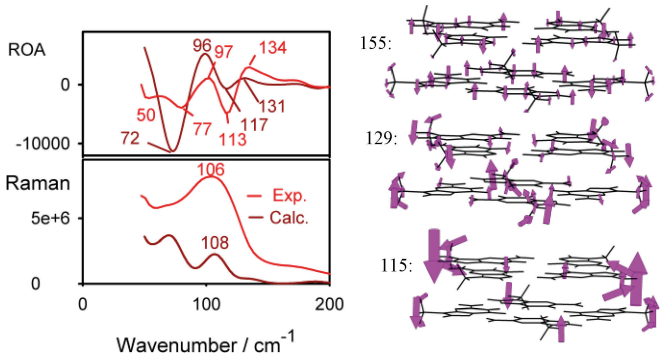

Figure 4. Low-frequency ROA and Raman spectra: experiment for 500 mM $GMPK_2$, calculation for the M dimer (no ions, B3LYP/6-31G**/CPCM wavenumbers shifted by 10 cm^{-1} up), and examples of involved vibrational modes.

Regular Nonamer Model (Q_9)

Based on a direct DFT computation of a regular quadruplex trimer (B3LYP/6-31G**/CPCM) and subsequent transfer of the vibrational parameters, the resultant spectra plotted in Figure 5 very well reproduce the $GMPK_2$ experiment. After minor frequency adjustments (Table S2) most of the observed Raman bands can be assigned, with reasonable relative intensities. Inconsistencies appearing mostly within 1000–1400 cm^{-1} can be attributed to the high density of the vibrations in this region combined with DFT reproducing different vibrational frequencies (such as P=O stretching and CH bending) with different errors,[22] and lack of the dynamic and explicit solvent aspects in the modeling.

The computed ROA bands match the experimental ones namely in the base-vibrating regions (50–250 and 1300–1800 cm^{-1}). Above 1600 cm^{-1}, the calculated intensity for the CO stretching bands is too high, which can again be attributed to the lack of proper dynamics/solvent in the model. The very good agreement within 50–250 cm^{-1}, including correct ROA/Raman ratios, indicates that these modes are less affected by the dynamics and solvent. This is consistent with a rigid structure of the quadruplex and hydrophobic character of the bases, in addition shielded from the environment by the sugar-phosphate residues.

Within 250–1300 cm^{-1} the ROA signal is not well reproduced. In particular, the bands around 400 cm^{-1} are clearly calculated with wrong signs. The sugar-phosphate residue often participates in vibrations at this region, which suggests that its conformation in the rigid model is wrong, or that specific solvent-solute interactions and the dynamics play a significant role. Indeed, for monomeric GMP, much better results were obtained by extensive averaging of solvent-solute clusters;[22] this is not possible for us for the larger quadruplex.

Averaging of MD Snapshots

The snapshots were created for quadruplex dodecamer; vibrational parameters were calculated using DFT for a central dimmer and transferred to six central quadruplex residues. Three structures were tried, named according the sugar puckering, an "SN" one according to an NMR model,[8] and more regular "S" and "N" sequences (Table S3). In Figure 6 we can see that this approach leads to a more realistic Raman band shapes than for Q_9, with high similarities (0.85–0.88) to the experiment. However, the Raman quadruplex spectra do not much differ from those simulated for monomeric GMP.[22]

The benefit of MD modeling compared to the regular Q_9 nonamer is not so clear for ROA; in particular the N and SN geometries gives a very poor representation of the experimental data, with negative similarity indices. Only the S structure gives a positive one, with mostly the right sign patterns in the base-dominated regions (below 250 and above 1300 cm^{-1}). In the CH stretching region (Figure S6) all MD models approximately reproduce the predominantly positive signal in ROA experiment. The mediocre performance of MD is not surprising as there is nor reliable force field usable for the metal coordination bonds and other complex interactions.

Further tests revealed that sodium in place of potassium give quite similar spectra for the MD modeling approach (Figure S4). The low-frequency ROA pattern also appeared to be quite sensitive to the polymer length. While the higher-frequency parts of the spectra are almost identical for quadruplex trimer and nonamer, there are still some changes below 250 cm^{-1} (Figure S5).

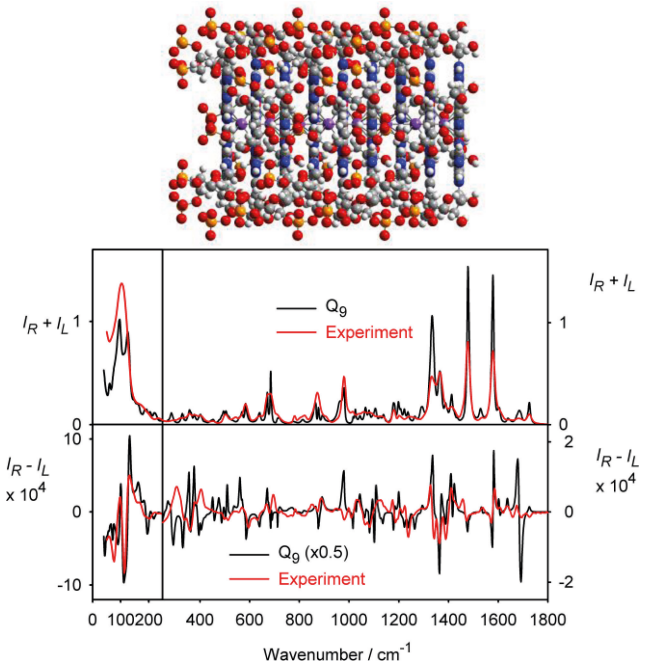

Figure 5. A regular nonamer structure, its calculated Raman and ROA spectra, and the 500 mM $GMPK_2$ experiment. In the calculation, vibrational frequencies were adjusted according to Table S2 and the intensities scaled by one factor to reproduce experimental Raman integral intensity within 300–1900 cm^{-1}.

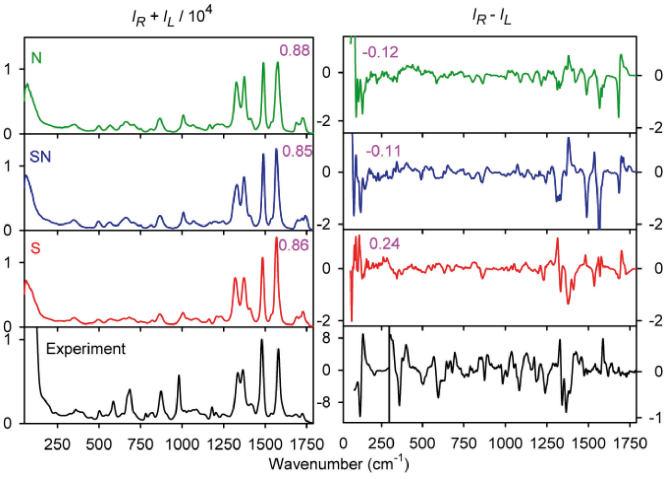

Figure 6. Spectra simulated for three MD dodecamer models (SN=Wu's NMR structure,[8] and two structures with regular (S/N) GMP conformations, averages of 20 MD snapshots) and the experiment. The similarity indices σ (overlap integrals within 300.. 1800 cm^{-1} of normalized experimental and calculated spectra) are indicated in magenta.

The MD results are consistent with the twist analyses for the M simplified dimer (Figure S3), indicating that the twist between adjacent GMP quartets should be above 45°. Indeed, in the SN structure $\tau = 33°$, while for N and S $\tau = 63°$ and 48°, respectively (Table S3). These values are close to the best one $\tau = 64°$ found for the M dimer based on the similarity of its spectra with the experiment, or $\tau = 60°$used in the nonamer model. They are also in a good agreement with the profile of the free energy obtained for a dimer formed of two GMP quartets where, according to the MD WHAM, angles around 64° are favored (Figure 7). We can thus conclude that ROA spectra suggest that the GMP aggregates in the presence of potassium forms S-type aggregates with the most probable twist of ~64°.

Conclusions

We found that high GMP concentrations produce distinct Raman and ROA spectral changes that could be related to quadruplex formation. In particular, the ROA spectra appeared quite informative, which could open applications of this technique in the field of quadruplexes, but also for general research of nucleic acids. Very useful appears the low-frequency (< 250 cm^{-1}) signal, which is relatively easy to detect and stems primarily from the interactions of neighboring GMP quartets and their out-of-plane deformation vibrations. Similarly, within ~1450–1800 cm^{-1} ROA intensities of in-plane C=C, C=N and C=O stretching vibrations are almost entirely dependent of the twist between the quadruplex GMP quartets.

The spectra simulations were extremely helpful for the spectra interpretation and in principle can provide an unambiguous confirmation of the quadruplex structure in solutions. Unfortunately, they are presently hampered by the size of the systems, variability of the vibrations involved, and complexity of the interactions. Current MD force fields do not appear fit to describe the combined electrostatic-covalent character of the metals coordinated to GMP. In addition, we cannot exclude that multiple structures are present in the sample, e.g., GMP dimers, apart from regular quadruplex polymers. However, the comparison of our experimental Raman spectra with those obtained for oligomeric quadruplexes indicates that mononucleotide quadruplexes highly prevailed.

In spite of these problems, we could determine the most probable GMP quadruplex structure, in particular the twist between neighboring quartets, assign the most prominent spectra features to the underlying vibrational motions, and point out the principle differences between sodium and potassium if interacting with GMP. In the future, greater variability of experimental conditions may reveal more details about the molecular interactions, while improvement of the computational methodology is also desirable for a more precise description of structure and dynamics of the nucleic acid components.

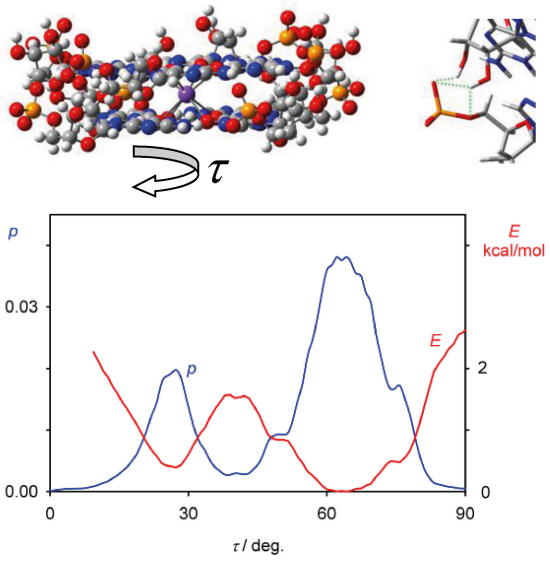

Figure 7. Twist probability (p) and free energy (E) computed for a quadruplex dimer by the WHAM method. Above: random snapshot geometry and detail of the H-bonding (in green) for τ ~60°, presumably stabilizing this twist value.

Experimental Section

Spectra Measurement

Disodium salt and free acid of guanosine 5′-monophosphate (GMP) were purchased from Merck. Potassium salt was made by titration of the acid with KOH to pH ~8.5 and lyophilization. Three samples were prepared by dissolution in deionized water to the concentrations of 763 mM (sodium salt), 500 mM (potassium salt), and 610 mol/L (sodium salt) with KCl to a total concentration of 200 mM. Temperature-dependent Raman and ROA spectra in a range of 50–4500 cm^{-1}were recorded on a spectrometer constructed at the Palacký University Olomouc operating with 532 nm excitation wavelength.[27] The experiments were performed at the scattered circular polarization (SCP) modulation and backscattering geometry (180°), the samples were held in a fused silica cell of 4 mm optical path length (3 mm width, 70 µl volume), illumination time was set to 0.5 s and spectral resolution was 8 cm^{-1}. Laser power at the sample was 800 mW, 7–10 temperature cycles were measured, total acquisition times for each temperature were 1–5 hours. From Raman spectra solvent (H_2O) signal was subtracted, and minor baseline corrections made. The intensity units are detected electrons per wavenumber interval per irradiation energy (cm J^{-1}) normalized to molar concentration of GMP monomers.

Rigid DFT Models

A simpler model dimer M composed of eight 9-methylguanines was investigated first (Figure 2), i.e., the sugar-phosphate residues were replaced by methyls. Relaxed scans were performed to obtain the dependence of the electronic energy on the distance d and twist τ. The D_4 and C_4 point group symmetries for the two stacking modes were kept, and the B3LYP[28]/6-31G**/CPCM[29](H_2O)/GD3BJ[30] level was applied as implemented in the Gaussian program.[31] Examples Gaussian inputs in internal coordinates for this and similar rigid models are given at the end of the Supporting Information. The M dimers were investigated without metals, with Na^+ and K^+ ions in the quadruplex planes, and with one Na^+ and K^+ atom in the middle. For the equilibrium structures the geometry was fully optimized and Raman and ROA spectra generated with a larger, 6–

311++G** basis set, otherwise using the same parameters as for the PES scans.

Similarly, symmetrized (C_4) geometry of GMP quadruplex trimer including the sugar-phosphates was optimized at the same level (6-31G** basis set, 434 atoms) using fixed twist of 60°, and harmonic vibrational frequencies. Raman and ROA intensities calculated by Gaussian. Relaxed structures, different twists (55,65 70°) or functionals (B97D) provided inferior results and are not shown. Two potassium atoms were kept between the quadruplex planes. The optimized geometry was propagated to create quadruplex nonamer (Figure 5), spectra of which were calculated using the Cartesian coordinate-based tensor transfer (CCT)[23] of vibrational parameters calculated for the trimer.

From the line intensities, smooth spectra were simulated using Lorentzian profiles of full width at half height of 10 cm^{-1}. The Raman and ROA intensities were scaled by one factor, to provide the same Raman integral intensity as the experiment.

Molecular Dynamics

MD was performed within the Amber 18 software.[32] The TIP3P[33] force field was used for water; the GAFF, GAFF2[34] RNA.OL3[35] and DNA.Bsc1[36] force fields were tried for GMP, partial atomic charges were calculated[37] at the CPCM–B3LYP/6-31++G(d,p) level of theory. The DNA.Bsc1 force field provided the best results and was used as default. Previously, DNA.Bsc1 gave reasonable ROA and Raman spectra of GMP monomer;[22] in addition, we observed that the other force fields sometimes predicted too short hydrogen bond lengths.

NVT dynamics was performed at 300 K using 1 fs integration step. First, the solvated systems were equilibrated for 1 ns, subsequent production run was carried out for 200 ns, snapshots were selected in regular intervals. A cutoff of 8 Å was used for the non-covalent interactions, the temperature was controlled by the Langevin thermostat (collision frequency 2 ps^{-1}).[38]

Monomer GMP spectra in solution were simulated using a combination of molecular dynamics (MD) and density functional theory (DFT) as described previously.[22] Quadruplex dodecamers (48 GMP molecules) were investigated trying three starting conformations, an NMR-derived geometry proposed by Wu,[8] where the "S" and "N" GMP conformers oscillate in individual GMP quartets, and uniform S and N ones. For simplicity, we keep the S/N notation, although ideal S/N parameters had to be modified to avoid atom overlap in the quadruplex polyme (Table S3). The 12-mers were placed in a 64^3 $Å^3$ cubic box, otherwise filled with water molecules and potassium counterions. After an equilibration phase, 200 ns production run was performed.

Using MD snapshot geometries of the 12-mer, middle quadruplex dimers without water molecules were partially optimized in the normal mode coordinates,[39] harmonic force field and polarizability derivatives were calculated at the B3LYP/6-31G**/CPCM(H_2O)/GD3BJ level by Gaussian. Using the CCT method, vibrational parameters were transferred from the dimmers to quadruplex hexamers. These were made from the quadruplexes close to the middle of the 12-mer, to minimize the effects of the more irregular termini. The spectra thus obtained were averaged for 20 snapshots for each structure (S, N, SN) investigated.

Smaller MD models consisted of two G-quartets (8 GMPs); here the weighted histogram analysis method (WHAM)[40] was performed to investigate the dependence of the free energy on mutual twist of the G-quartets.

Acknowledgements

The work was supported by the Grant Agency of the Czech Republic (22-04669S) and the Charles University Grant Agency (22224 and 298123). Computational resources were provided by the project "e-INFRA CZ" (e-INFRA LM2018140). Open Access publishing facilitated by Ustav organicke chemie a biochemie Akademie ved Ceske republiky, as part of the Wiley - CzechELib agreement.

Conflict of Interests

JK is involved in commercialization of an ROA spectrometer. The other authors declare no conflict of interest.

Data Availability Statement

The data that support the findings of this study are available in the supplementary material of this article.

Keywords: Guanine quadruplexes · Density functional theory · Molecular dynamics · Raman optical activity

[1] M. Gellert, M. N. Lipsett, D. R. Davies, *Proc. Natl. Acad. Sci. U.S.A* **1962**, *48*, 2013–2018.
[2] a) V. Sasisekharan, S. Zimmerman, D. R. Davies, *J. Mol. Biol.* **1975**, *92*, 171–179; b) J. Chantot, W. Guschlbauer, *FEBS Letters* **1969**, *4*, 173–176; c) T. Simonsson, *Biol. Chem.* **2001**, *382*, 621–628.
[3] J. T. Davis, *Angew. Chem. Int. Ed.* **2004**, *43*, 668–698.
[4] G. S. Oxford, R. G. Gillespie, *Annu. Rev. Entomol.* **1998**, *43*, 619–643.
[5] R. H. Douglas, J. C. Partridge, N. J. Marshall, *Prog. Retinal Eye Res.* **1998**, *17*, 597–636.
[6] J. Teyssier, S. V. Saenko, D. van der Marel, M. C. Milinkovitch, *Nat. Commun.* **2015**, *6*, 6368.
[7] a) J. M. Lehn, *Science* **2002**, *295*, 2400–2403; b) D. Gur, B. A. Palmer, S. Weiner and L. Addadi, *Adv. Funct. Mater.* **2017**, *27*, 1603514.
[8] G. Wu, I. C. M. Kwan, *J. Am. Chem. Soc.* **2009**, *131*, 3180–3182.
[9] a) K. J. Neurohr, H. H. Mantsch, *Can. J. Chem.* **1979**, *57*, 1986–1994; b) J. B. Hightower, D. R. Olmos, J. A. Walmsley, *J. Phys. Chem. B* **2009**, *113*, 12214–12219.
[10] a) Z. Zhang, S. J. Kim, B. L. Gaffney, R. A. Jones, *J. Am. Chem. Soc.* **2006**, *128*, 7015–7024; b) S. Nakayama, I. Kelsey, J. Wang, H. O. Sintim, *Chem. Commun.* **2011**, *47*, 4766–4768; c) J. Novotná, I. Goncharova, M. Urbanová, *Supramol. Chem.* **2014**, *26*, 7–14.
[11] a) J. Novotná, I. Goncharova, *Chirality* **2012**, *24*, 432–438; b) K. Mudroňová, V. Římal, P. Mojzeš, *Vib. Spectrosc.* **2016**, *82*, 60–65; c) V. Setnička, M. Urbanová, K. Volka, S. Nampally, J. M. Lehn, *Chemistry* **2006**, *12*, 8735–8743.
[12] S. Yamamoto, S. Ishiro, J. Kessler, P. Bouř, *Phys. Chem. Chem. Phys.* **2021**, *23*, 26501–26509.
[13] J. Kessler, J. Kapitán, P. Bouř, *J. Phys. Chem. Lett.* **2015**, *6*, 3314–3319.
[14] P. Michal, J. Kapitán, J. Kessler, P. Bouř, *Phys. Chem. Chem. Phys.* **2022**, *24*, 19722–19733.
[15] L. Nafie, *Vibrational Optical Activity: Principles and Applications*, Wiley, Chichester, **2011**.
[16] a) L. D. Barron, M. P. Bogaard, A. D. Buckingham, *J. Am. Chem. Soc.* **1973**, *95*, 603–605; b) J. Šebestík, P. Bouř, *J. Phys. Chem. Lett.* **2011**, *2*, 498–502; c) M. Spasovová, J. Kapitán, Š. Jílek, M. S. ParaKkadan, J. Klener, N. S. Lynn, V. Kopecký, V. Baumruk, V. Profant, *Spectrochim. Acta A Mol. Biomol. Spectrosc.* **2024**, *313*, 124119.
[17] S. Yamamoto, M. Straka, H. Watarai, P. Bouř, *Phys. Chem. Chem. Phys.* **2010**, *12*, 11021–11032.
[18] L. D. Barron, E. W. Blanch, L. Hecht, *Adv. Protein Chem.* **2002**, *62*, 51–90.
[19] A. F. Bell, L. Hecht, L. D. Barron, *J. Am. Chem. Soc.* **1994**, *116*, 5155–5161.

[20] a) A. F. Bell, L. Hecht, L. D. Barron, *J. Chem. Soc., Faraday Trans.* **1997**, *93*, 553–562; b) A. F. Bell, L. Hecht, L. D. Barron, *J. Am. Chem. Soc.* **1998**, *120*, 5820–5821; c) E. W. Blanch, L. Hecht, C. D. Syme, V. Volpetti, G. P. Lomonossoff, K. Nielsen, L. D. Barron, *J. Gen. Virol.* **2002**, *83*, 2593–2600.
[21] a) M. Pecul, E. Lamparska, C. Capelli, L. Frediani, K. Ruud, *J. Phys. Chem. A* **2006**, *110*, 2807–2815; b) K. H. Hopmann, K. Ruud, M. Pecul, A. Kudelski, M. Dračínský, P. Bouř, *J. Phys. Chem. B* **2011**, *115*, 4128–4137.
[22] V. Schrenková, M. S. Para Kkadan, J. Kessler, J. Kapitán, P. Bouř, *Phys. Chem. Chem. Phys.* **2023**, *25*, 8198–8208.
[23] a) S. Yamamoto, X. Li, K. Ruud, P. Bouř, *J. Chem. Theory Comput.* **2012**, *8*, 977–985; b) P. Bouř, J. Sopková, L. Bednárová, P. Maloň, T. A. Keiderling, *J. Comput. Chem.* **1997**, *18*, 646–659.
[24] J. M. Benevides, S. A. Overman, G. J. Thomas, *J. Raman Spectrosc.* **2005**, *36*, 279–299.
[25] a) G. Holzwarth, I. Chabay, *J. Chem. Phys.* **1972**, *57*, 1632–1635; b) P. Bouř, T. A. Keiderling, *J. Am. Chem. Soc.* **1992**, *114*, 9100–9105.
[26] L. D. Barron, *Molecular Light Scattering and Optical Activity*, Cambridge University Press, Cambridge, UK, **2004**.
[27] P. Michal, R. Čelechovský, M. Dudka, J. Kapitán, M. Vůjtek, M. Berešová, J. Šebestík, K. Thangavel, P. Bouř, *J. Phys. Chem. B* **2019**, *123*, 2147–2156.
[28] A. D. Becke, *J. Chem. Phys.* **1993**, *98*, 5648–5652.
[29] A. Klamt, in *COSMO and COSMO-RS*, Vol. 1 Eds.: P. R. Schleyer, N. L. Allinger, T. Clark, J. Gasteiger, P. A. Kollman, H. F. Schaefer III and P. R. Schreiner), John Wiley & Sons, Chichester, **1998**, 604–615.
[30] S. Grimme, S. Ehrlich, L. Goerigk, *J. Comput. Chem.* **2011**, *32*, 1456–1465.
[31] M. J. Frisch, G. W. Trucks, H. B. Schlegel, G. E. Scuseria, M. A. Robb, J. R. Cheeseman, G. Scalmani, V. Barone, G. A. Petersson, H. Nakatsuji, X. Li, M. Caricato, A. V. Marenich, J. Bloino, B. G. Janesko, R. Gomperts, B. Mennucci, H. P. Hratchian, J. V. Ortiz, A. F. Izmaylov, J. L. Sonnenberg, D. Williams-Young, F. Ding, F. Lipparini, F. Egidi, J. Goings, B. Peng, A. Petrone, T. Henderson, D. Ranasinghe, V. G. Zakrzewski, J. Gao, N. Rega, G. Zheng, W. Liang, M. Hada, M. Ehara, K. Toyota, R. Fukuda, J. Hasegawa, M. Ishida, T. Nakajima, Y. Honda, O. Kitao, H. Nakai, T. Vreven, K. Throssell, J. A. Montgomery Jr., J. E. Peralta, F. Ogliaro, M. J. Bearpark, J. J. Heyd, E. N. Brothers, K. N. Kudin, V. N. Staroverov, T. A. Keith, R. Kobayashi, J. Normand, K. Raghavachari, A. P. Rendell, J. C. Burant, S. S. Iyengar, J. Tomasi, M. Cossi, J. M. Millam, M. Klene, C. Adamo, R. Cammi, J. W. Ochterski, R. L. Martin, K. Morokuma, O. Farkas, J. B. Foresman and D. J. Fox, in Gaussian 16 Rev. A.03, Vol. Gaussian, Inc., Wallingford, CT, **2016**.
[32] D. A. Pearlman, D. A. Case, J. W. Caldwell, W. S. Ross, T. E. Cheatham, S. Debolt, D. M. Ferguson, G. Seibel, P. A. Kollman, *Comp. Phys. Commun.* **1995**, *91*, 1–41.
[33] W. L. Jorgensen, J. Chandrasekhar, J. D. Madura, *J. Chem. Phys.* **1983**, *79*, 926–935.
[34] W. D. Cornell, P. Cieplak, C. I. Bayly, I. R. Gould, K. M. Merz, D. M. Ferguson, D. C. Spellmeyer, T. Fox, J. W. Caldwell, P. A. Kollman, *J. Am. Chem. Soc.* **1995**, *117*, 5179–5197.
[35] M. Zgarbová, M. Otyepka, J. Šponer, A. Mládek, P. Banáš, T. E. Cheatham III, P. Jurečka, *J. Chem. Theory Comput.* **2011**, *7*, 2886–2902.
[36] I. Ivani, P. D. Dans, A. Noy, A. Pérez, I. Faustino, A. Hospital, J. Walther, P. Andrio, R. Goñi, A. Balaceanu, G. Portella, F. Battistini, J. L. Gelpí, C. González, M. Vendruscolo, C. A. Laughton, S. A. Harris, D. A. Case, M. Orozco, *Nat. Methods* **2016**, *13*, 55–58.
[37] R. Aduri, B. T. Psciuk, P. Saro, H. Taniga, H. B. Schlegel, J. SantaLucia, *J. Chem. Theory Comput.* **2007**, *3*, 1464–1475.
[38] J. Liu, D. Li, X. Liu, *J. Chem. Phys.* **2016**, *145*, 024103.
[39] a) P. Bouř, T. A. Keiderling, *J. Chem. Phys.* **2002**, *117*, 4126–4132; b) P. Bouř, *Collect. Czech. Chem. Commun.* **2005**, *70*, 1315–1340.
[40] S. Kumar, D. Bouzida, R. H. Swendsen, P. A. Kollman, J. M. Rosenberg, *J. Comput. Chem.* **1992**, *13*, 1011–1021.

Manuscript received: September 11, 2024
Accepted manuscript online: September 27, 2024
Version of record online: November 6, 2024